Ecotoxicology and Environmental Safety 193 (2020) 110348

Contents lists available at ScienceDirect

Ecotoxicology and Environmental Safety

journal homepage: www.elsevier.com/locate/ecoenv

Evaluation of cytotoxicity, apoptosis, and genotoxicity induced by indium chloride in macrophages through mitochondrial dysfunction and reactive oxygen species generation

Ping-Kun Tsai[a,b], Sheng-Wen Wu[c,d], Chen-Yu Chiang[e,f,g], Min-Wei Lee[e,f,h], Hung-Yi Chen[i], Wen-Ying Chen[g], Chun-Jung Chen[j], Shun-Fa Yang[a,k], Chao-Bin Yeh[a,d,l,1], Yu-Hsiang Kuan[e,f,*,1]

[a] Institute of Medicine, Chung Shan Medical University, Taichung, Taiwan
[b] Department of Internal Medicine, Zuoying Branch of Kaohsiung Armed Forces General Hospital, Kaohsiung, Taiwan
[c] Division of Nephrology, Chung Shan Medical University Hospital, Taichung, Taiwan
[d] The School of Medicine, Chung Shan Medical University, Taichung, Taiwan
[e] Department of Pharmacology, School of Medicine, Chung Shan Medical University, Taichung, Taiwan
[f] Department of Pharmacy, Chung Shan Medical University Hospital, Taichung, Taiwan
[g] Department of Veterinary Medicine, National Chung Hsing University, Taichung, Taiwan
[h] A Graduate Institute of Microbiology and Public Health, National Chung Hsing University, Taichung, Taiwan
[i] School of Pharmacy, China Medical University, Taichung, Taiwan
[j] Department of Education and Research, Taichung Veterans General Hospital, Taichung, Taiwan
[k] Department of Medical Research, Chung Shan Medical University Hospital, Taichung, Taiwan
[l] Department of Emergency Medicine, Chung Shan Medical University Hospital, Taichung, Taiwan

ARTICLE INFO

Keywords:
$InCl_3$
Macrophages
Apoptosis
Genotoxicity
Mitochondrial dysfunction
ROS generation

ABSTRACT

Due to rapid advances in the era of electronic technologies, indium has played the important material for the production of liquid crystal display screens in the semiconductor and optoelectronic industries. The present study focuses on evaluating the toxic effects and related mechanisms of indium chloride ($InCl_3$) on RAW264.7 macrophages. Cytotoxicity was induced by $InCl_3$ in a concentration- and time-dependent manner. $InCl_3$ had the ability to induce macrophage death through apoptosis rather than through necrosis. According to the cytokinesis-block micronucleus assay and alkaline single-cell gel electrophoresis assay, $InCl_3$ induced DNA damage, also called genotoxicity, in a concentration-dependent manner. Cysteine-dependent aspartate-directed protease (caspase)-3, −8, and −9 were activated by $InCl_3$ in a concentration-dependent manner. Mitochondria dysfunction and cytochrome *c* release from the mitochondria were induced by $InCl_3$ in a concentration-dependent manner. Downregulation of BCL2 and upregulation of BAD were induced by $InCl_3$ in a concentration-dependent manner. More, we proposed that $InCl_3$ treatment generated reactive oxygen species (ROS) in a concentration-dependent manner. In conclusion, the current study revealed that $InCl_3$ induced macrophage cytotoxicity, apoptosis, and genotoxicity via a mitochondria-dependent apoptotic pathway and ROS generation.

1. Introduction

Indium is a rare metal element with abundance of approximately 0.05–0.20 parts per million in the Earth's crust. Indium has soft, ductile, malleable, lustrous features and belongs to Group 3 A elements of the periodic table (Phipps et al., 2008). Indium is widely used in high-tech semiconductor and optoelectronic industries for the production of indium tin oxide (ITO) films (Li et al., 2011). ITO films are key components of liquid crystal display (LCD) screens, which have extensive applications in computers, laptops, mobile phones, sensor modules, photovoltaic cells, and televisions (Wang, 2011; Zhang et al., 2015). The ITO film is a mixture of 90% indium oxide and 10% tin oxide. Indium oxide is generated by the reaction between indium chloride ($InCl_3$) and $NH_3{\cdot}H_2O$ under high temperature and pressure (Zhang et al., 2015). Therefore, workers in ITO film manufacturing are at risk of overexposure to indium and related substances, especially

* Corresponding author. Department of Pharmacology , School of Medicine, Chung Shan Medical University and Chung Shan Medical University Hospital, No.110, Sec. 1, Jianguo N. Rd., Taichung, 402, Taiwan.
E-mail address: kuanyh@csmu.edu.tw (Y.-H. Kuan).
[1] These two authors have equal contributions to the study.

https://doi.org/10.1016/j.ecoenv.2020.110348
Received 28 September 2019; Received in revised form 13 February 2020; Accepted 15 February 2020
Available online 27 February 2020

exposure to $InCl_3$ through inhalation (Chonan et al., 2019).

Precise knowledge regarding the toxic effects of indium and related substances on humans and animals is now available. Indium lung, pneumotoxic effects, inhalation carcinogenicity, and chronic toxicity induced by ITO have been shown in humans and in rat and mouse models (Chonan et al., 2019; Chen et al., 2019; Nagano et al., 2011). A zebrafish model has also been used to demonstrate the toxic effect of indium in developmental and behavioral assays (Olivares et al., 2016). The intratracheal-administration hamster model, indium oxide has been shown to cause pulmonary toxicity similar to ITO (Tanaka et al., 2010; Bomhard, 2018). In vitro studies have also proposed that ITO and indium oxide could evoke mutagenicity and genotoxicity based on the results of the revised bacterial reverse mutation assay (Ames test), Bhas 42 cell transformation assay, and micronucleus (MN) test (Akyıl et al., 2016; Hasegawa et al., 2012; Bomhard, 2018). Both indium oxide and ITO induce cytotoxicity and proinflammatory responses in macrophages (Olgun et al., 2017; Badding et al., 2015). However, the toxic effect of $InCl_3$, which is the main source of ITO and indium oxide, on macrophages is unclear. In the current study, we investigated the hypothesis that $InCl_3$ induces cytotoxicity, apoptosis, and genotoxicity in RAW264.7 macrophages through intracellular reactive oxygen species (ROS) production and mitochondria-dependent apoptotic pathway.

2. Materials and methods

2.1. Materials

Dulbecco's Modified Eagle Medium (DMEM), streptomycin, anfotericina B, and penicillin were obtained from Hyclone (Logan, UT, USA). Fetal bovine serum (FBS) was purchased from Gibico-BRL (Gaithersburg, USA). Cysteine-dependent aspartate-directed protease (caspase) fluorometric assay kits were obtained from Enzo Life Sciences (Plymouth Meeting, PA, USA). Annexin V-fluorescein isothiocyanate/propidium iodide (FITC/PI) assay kits were obtained from BioVision (San Jose, CA, USA). Low melting agarose and normal-melting-point agarose was purchased from. LONZA (Rockland, ME, USA). True-Nuclear Transcription Factor Buffer Set and FITC anti-cytochrome *c* antibody were purchased from BioLegend (San Diego, CA, USA). BAD, BCL-2, and β-actin were purchased from Santa Cruz Biotechnology (St Louis, MO, USA) $InCl_3$, dichlorofluorescin diacetate (DCFH-DA), dimethyl sulfoxide (DMSO), 3-(4,5-dimethylthiazol-2-yl)-2,5-diphenyl tetrazolium bromide (MTT), and other reagents, unless specifically stated, were purchased from Sigma-Aldrich (St. Louis, MO).

2.2. Cell line, cell culture, and cell treatment

Murine RAW264.7 macrophages used in the present study were purchased from the Bioresource Collection and Research Centre (Hsinchu, Taiwan). RAW264.7 cells were cultured in DMEM supplemented with 10% fetal bovine serum and 1% penicillin/streptomycin/fungizone in a humidified incubator with 5% CO_2 at 37 °C. After passaging, RAW264.7 cells were seeded into culture plates. After 24 h, the cells were treated with $InCl_3$ at concentrations of 0, 1, 10, and 50 μM for 6, 12, 24, and 48 h (Huang et al., 2019).

2.3. Cell viability assay

The effect of $InCl_3$ on the viability of RAW264.7 cells was evaluated using the MTT assay (Chien et al., 2018). After treatment, the medium was substituted with serum-free medium containing 0.5 mg/mL MTT for 2 h at 37 °C. After the supernatant was discarded, the purple formazan crystals in the cells were extracted with DMSO. The absorbance of the plates was measured on a microplate reader (Synergy HT Multi-Mode Microplate Reader, Biotek, Winooski, VT) at 550 nm wavelength.

2.4. Flow cytometric analysis of necrosis and apoptosis

Detection of $InCl_3$-induced necrosis and apoptosis was performed on the Accuri™ C6 flow cytometer (BD Biosciences, San Jose, CA, USA) using a commercially available annexin V-FITC/PI apoptosis detection kit. After the cells were treated with $InCl_3$ at the indicated concentrations for 24 h, apoptosis and necrosis were identified through annexin V-FITC/PI staining, as described previously (Chien et al., 2018). The proportions of viable, apoptotic, and necrotic RAW264.7 cells were distributed into the phases of annexin V negative and PI negative, annexin V positive and PI negative, and annexin V positive and PI positive cells, respectively.

2.5. Alkaline single-cell gel electrophoresis assay

$InCl_3$-induced DNA single-strand breaks were detected using the alkaline single-cell gel electrophoresis assay (comet assay), as previously described (Huang et al., 2018). In brief, the cells were treated with $InCl_3$ at the indicated concentrations or H_2O_2 at 50 μM for 24 h. After collection had been completed, the cells were incubated with 1% low-melting agarose and then placed on microscope slides that were precoated with 1% normal-melting-point agarose. After solidification of the gel on ice, the slides immersed in cold lysis solution (2.5 M NaCl, 100 mM EDTA, 10 mM Tris-HCl, 1% Tritron X-100, 200 mM NaOH, 34.1 mM N-lauroyl-sarcosine, and 10% DMSO, pH 10) for 1 h. After washing the slides three times in PBS, the slides were then placed in a horizontal electrophoresis chamber containing freshly prepared electrophoresis buffer (1 mM Na_2EDTA, 300 mM NaOH, pH $>$ 13). After electrophoresis, the slides were stained with 20 μg/mL ethidium bromide and then observed through fluorescence microscopy (Nikon, Tokyo, Japan). DNA damage was analyzed using the image analysis system Comet v.3 (Kinetic Imaging Ltd., Liverpool, UK), which calculated the tail length and tail moment. The tail length calculated the distance from the head centre to the end of the tail. The tail moment was calculated as tail length, multiply by percentage of DNA in the tail.

2.6. Cytokinesis-block micronucleus assay

$InCl_3$-induced DNA damage was detected using the alkaline comet assay, as previously described (Lee et al., 2018). After the cells were treated with $InCl_3$ at the indicated concentrations, H_2O_2 at 50 μM, or cytochalasin B at 3 mg/mL for 24 h, the cells were resuspended in 75 mM potassium chloride and then fixed with glacial acetic acid and methanol. The cells were seeded onto slides, air dried, and stained using Giemsa's solution.

2.7. Caspase activity assay

The effect of $InCl_3$ on caspase-3, -8, and -9 activity was evaluated using a caspase fluorometric assay kit, as previously described (Huang et al., 2018). The cell protein extracts from each sample were reacted with the fluorogenic substrates of caspase-3, -8, and -9 (Huang et al., 2018). The fluorescence intensity of each sample was measured on a fluorescence microplate reader at an excitation wavelength of 400 nm and an emission wavelength of 505 nm. Fluorescence intensity is expressed as a relative fluorescence unit (RFU).

2.8. Mitochondrial membrane potential assay

$InCl_3$-induced mitochondria dysfunction was detected using the mitochondrial membrane potential assay dye JC-1, as previously described (Lee et al., 2018). The cells were stained with JC-1 at 37 °C for 30 min after the cells were treated with $InCl_3$ at the indicated concentrations for 24 h. After being washed, the cells were immediately analyzed using the Accuri™ C6 flow cytometer. The proportions of the cells with mitochondrial dysfunction were distributed into groups of

red negative and green positive cells.

2.9. Measurement of cytochrome c release

After treatment, the cells were fixed and permeabilized using the True-Nuclear Transcription Factor Buffer Set. Once washed, the cells were incubated with FITC anti–cytochrome *c* antibody at room temperature for 1 h. The fluorescence intensity acquisition and analyses were performed with a BD Accuri C6 flow cytometer and corresponding software. Fluorescence intensity is expressed in RFU.

2.10. Western blot assay

The expression levels of BAD and BCL2 were assessed by Western blot assay as described previously (Huang et al., 2018). After treatment, the cells were washed with PBS and harvested in Western blot lysis solution. After centrifugation, the total protein concentration in the supernatant was calculated using the Bradford assay. Equal protein amounts of the lysates were separated using SDS-PAGE and electrophoretically transferred onto polyvinylidene difluoride membranes. The membranes were blocked by incubating them in 5% (w/v) skim milk for 1 h. After washing with PBS containing 0.1% Tween 20 (PBST), the membranes were incubated with the indicated primary antibodies including BAD, BCL2, and β-actin in PBST with 0.5% (w/v) skim milk for 2 h. After washing, the membranes were incubated with horseradish peroxidase-conjugated anti–mouse IgG secondary antibody in PBST with 0.5% (w/v) skim milk for 1 h. The blots were developed using ECL Western blotting reagents. ECL These Western blotting reagents were used to reveal the protein bands, and the Infinity CX5 system was applied to detect and quantify the bands.

2.11. Intracellular ROS generation

$InCl_3$-induced intracellular ROS generation was detected using the DCFH-DA fluorescence assay, as previously described (Lee et al., 2018). After treatment with $InCl_3$ at the indicated concentrations for 24 h, the cells were further incubated with DCFH-DA for 30 min. The fluorescence intensity of each sample was measured on the fluorescence microplate reader (Synergy HT Multi-Mode Microplate Reader, Biotek, Winooski, VT) at an excitation wavelength of 495 nm and an emission wavelength of 530 nm. Fluorescence intensity is expressed as a relative fluorescence unit (RFU).

2.12. Statistical analysis

Statistical analysis was performed using the statistical analysis software program SPSS (IBM, Chicago, IL, USA). All reported values are expressed as mean ± standard deviation. One-way analysis of variance followed by the Bonferroni *t*-test was conducted for multigroup comparison. *P* values less than 0.05 were considered significant for all tests.

3. Results

3.1. Effects of $InCl_3$ on the viability of RAW264.7 cells

In the cell viability assay, $InCl_3$ treatment for 3 h did not influence cell viability. However, subsequently, $InCl_3$ treatment for 12, 24, and 48 h reduced cell viability in a concentration-dependent manner. Additionally, treatment with $InCl_3$ at concentrations of 50, 1, and 1 μM for 12, 24, and 48 h began to reduce cell viability, respectively ($P < 0.05$, Fig. 1).

3.2. Effects of $InCl_3$ on types of cell death in RAW264.7 cells

To determine the type of cell death induced by $InCl_3$, the cells were analyzed by flow cytometry after annexin V-FITC/PI staining. Fig. 2 shows the representative results with an apparent shift of many cells into the annexin V-FITC positive region after treatment with $InCl_3$. These results demonstrated that $InCl_3$ induced apoptosis in a concentration-dependent manner, and that a significant increase was observed at 1 μM ($P < 0.05$, Fig. 2D). Moreover, cell necrosis was significantly induced by $InCl_3$ at a concentration of 50 μM ($P < 0.05$, Fig. 2B).

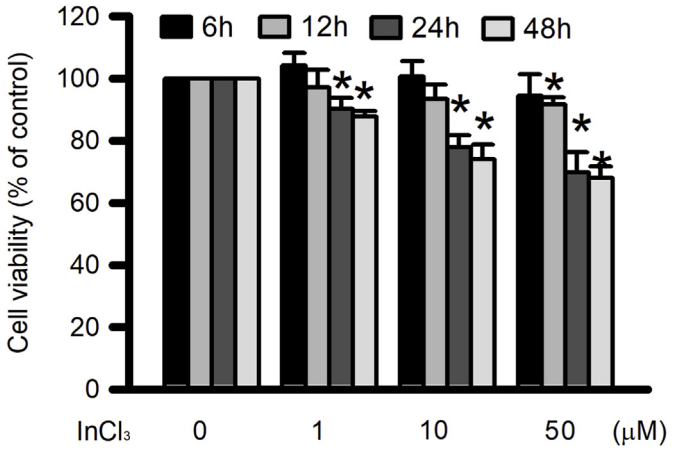

Fig. 1. $InCl_3$ induce cytotoxicity in RAW264.7 macrophages. The cell viability was measured by MTT colorimetric assay after treated with $InCl_3$ for 12, 24, or 48 h at 0, 1, 10, or 50 μM respectively. Values were expressed as a percentage of vehicle treated control group. Results are expressed as means ± SD (n = 4). *$P < 0.05$ considers significant as compare with control group, which indicated treatment with $InCl_3$ at 0 μM.

3.3. Effects of $InCl_3$ on genotoxicity in RAW264.7 cells

To determine the genotoxicity induced by $InCl_3$, DNA damage was analyzed through cytokinesis-block micronucleus and comet assays. The number of micronuclei induced by $InCl_3$ treatment for 24 h increased in a concentration-dependent manner, and a significant increase was observed at 5 μM ($P < 0.05$, Fig. 3). Furthermore, DNA single-strand breaks were induced by $InCl_3$ treatment for 24 h according to the comet assay (Fig. 4A). Statistically significant upregulation of tail moment (Fig. 4B) and tail length (Fig. 4C) was found between control cells and cells treated with $InCl_3$ at 10 and 50 μM ($P < 0.05$). These results indicated that $InCl_3$ induced genotoxicity in RAW264.7 cells in a concentration-dependent manner.

3.4. Effects of $InCl_3$ on caspase activity in RAW264.7 cells

To determine the activation of caspase-3, -8, and -9 induced by $InCl_3$, the cells were analyzed using the fluorometric caspase substrates Ac-DEVD-AFC, Ac-IETD-AFC, and Ac-LEHD-AFC, respectively. Detectable upregulation of caspase-3, -8, and -9 activities was induced by $InCl_3$ at 10 μM, and its stimulatory effect was concentration dependent ($P < 0.05$, Fig. 5).

3.5. Effects of $InCl_3$ on mitochondrial dysfunction in RAW264.7 cells

Mitochondrial dysfunction induced by $InCl_3$ was analyzed using the mitochondrial membrane potential assay dye JC-1. Mitochondria depolarization was induced by $InCl_3$ in a concentration-dependent manner, and a significant increase was observed at 10 μM ($P < 0.05$, Fig. 6).

3.6. Effects of $InCl_3$ on cytochrome c leakage in RAW264.7 cells

Leakage of cytochrome *c* from the mitochondria, which plays a

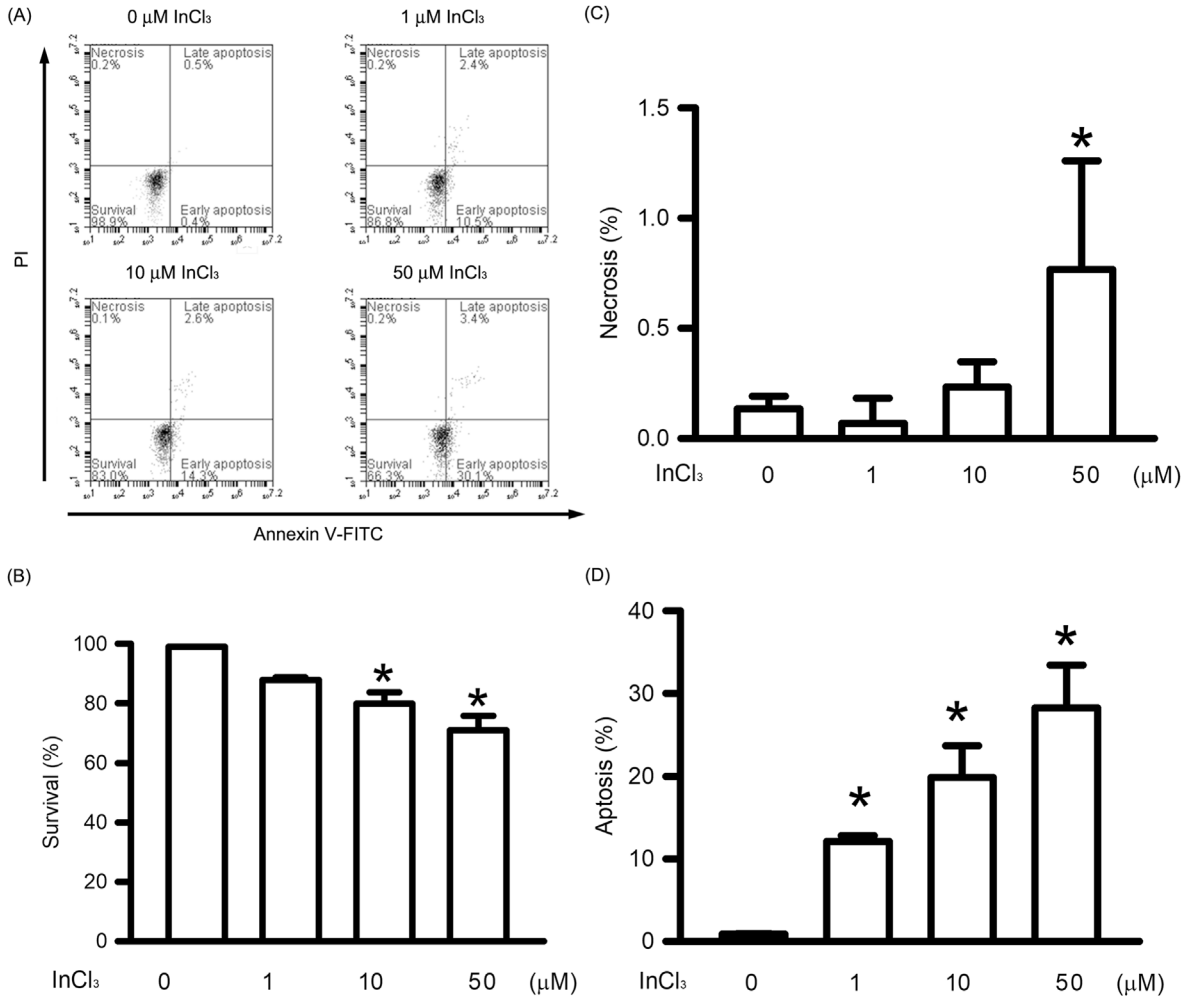

Fig. 2. $InCl_3$ induced apoptosis in RAW264.7 macrophages. The apoptosis was measured by Annexin V-FITC/PI assay kit using flowcytometry. (A) Cells were incubated with $InCl_3$ at various concentrations of 0, 1, 10, and 50 μM for 24 h at 37 °C. The upper left quadrant (Annexin V−/PI+) is representative of necrosis; upper right and lower right quadrants (Annexin V+/PI+ and Annexin V+/PI−) are representatives of apoptosis; and lower left quadrant (Annexin V−/PI−) is representative of living cells. Quantitatively the percentage of viable cells (B), necrotic cells (C), and apoptotic cells (D) were calculated and analyzed. Data are expressed as mean ± SD (n = 4). *$P < 0.05$ considers significant as compare with control group, which indicated treatment with $InCl_3$ at 0 μM.

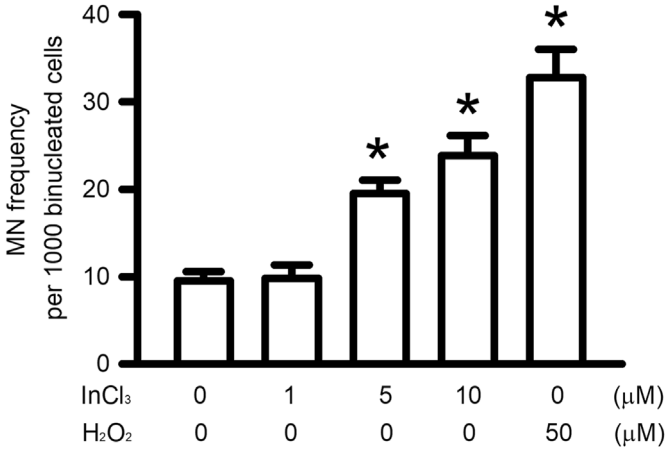

Fig. 3. $InCl_3$ induced formation of micronucleus in RAW264.7 macrophages. Data are expressed as mean ± SD (n = 4). *$P < 0.05$ considers significant as compare with control group, which indicated treatment with $InCl_3$ at 0 μM.

critical role in the mitochondria-mediated apoptotic pathway, was measured using a flow cytometer. Leakage of cytochrome *c* was induced by $InCl_3$ in a concentration-dependent manner, and a significant increase was observed at 10 μM ($P < 0.05$, Fig. 7).

3.7. Effects of $InCl_3$ on BAD and BCL2 expression in RAW264.7 cells

The expression of BAD and BCL2, which participates in the leakage of cytochrome *c*, was measured by Western blot assay. BAD expression was induced by $InCl_3$ in a concentration-dependent manner, and a significant increase was observed at 10 μM ($P < 0.05$). BAL2 expression was reduced by $InCl_3$ in a concentration-dependent manner, and a significant increase was observed at 10 μM ($P < 0.05$, Fig. 8).

3.8. Effects of $InCl_3$ on intracellular ROS generation in RAW264.7 cells

Intracellular ROS generation induced by $InCl_3$ was analyzed using the fluorescence assay dye DCFH-DA. $InCl_3$ induced intracellular ROS generation in the cells in a concentration-dependent manner, and a significant increase was observed at 1 μM ($P < 0.05$, Fig. 9).

4. Discussion

Indium is a rare, fusible, and ductile chemical element that exhibits properties and characteristics that are mostly intermediate between gallium and thallium. Indium is widely used today in the production of

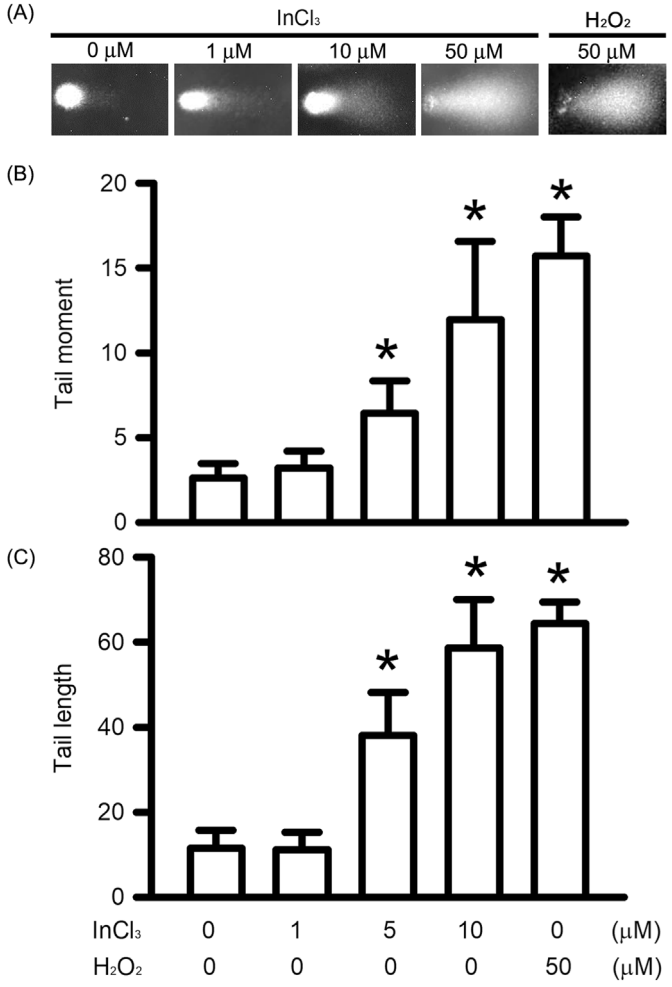

Fig. 4. $InCl_3$ induced genotoxicity in RAW264.7 macrophages via comet assay. (A) The gel electrophoresis for the cells treated with $InCl_3$ for 24 h at 0, 1, 10, or 50 μM and H_2O_2 for 24 h at 50 μM were shown. DNA damages were quantified as tail length (B) and tail moment (C). Data are expressed as mean ± SD (n = 4). *$P < 0.05$ considers significant as compare with control group, which indicated treatment with $InCl_3$ at 0 μM.

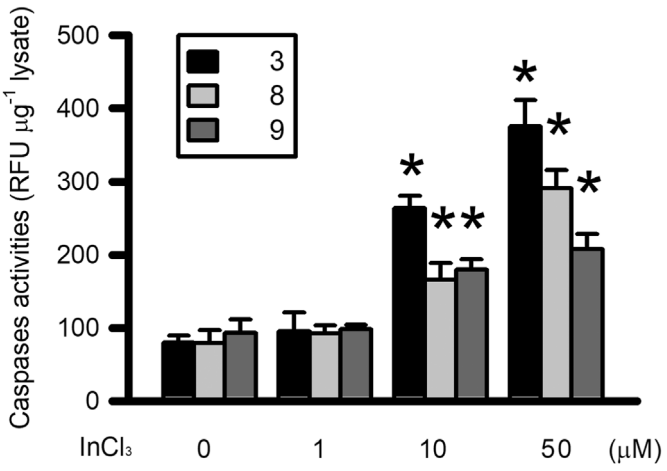

Fig. 5. $InCl_3$ induced activities of caspase-3, -8, and -9 in RAW264.7 macrophages. Data are expressed as mean ± SD (n = 4). *$P < 0.05$ considers significant as compare with control group, which indicated treatment with $InCl_3$ at 0 μM.

semiconductors and microelectronics. The amount of indium used has greatly increased in the past decade in parallel with manufacturing growth due to advances in technology. Occupational exposure to indium and related substances, including ITO, indium oxide, and $InCl_3$, predominately occurs through inhalation (Hines et al., 2013). Inhalation of indium and related substances can lead to the potentially fatal disease indium lung, which may include pulmonary toxicity and carcinogenicity, and the disease has been seen among workers involved in downstream industrial applications (Chonan et al., 2019; Lison, 2009; Nagano et al., 2011; Tanaka et al., 2010). Therefore, increased attention has been paid to the toxicity of indium and its related substances to humans (Hines et al., 2013). Macrophages play a key role in the innate immune system of lungs. Macrophages can uptake and solubilize indium-containing particles (InP) and ITO through phagolysosomal acidification, which then results in cytotoxicity and the release of indium ions (Gwinn et al., 2013). To correlate changes in InP- or ITO-treated mice through aspiration, pulmonary toxicity presents the same trend of cytotoxicity as that in macrophages (Gwinn et al., 2015). The ionic form of indium is the major primary cytotoxic component of indium-containing substances. Therefore, $InCl_3$ demonstrates greater cytotoxicity in macrophages than other indium-related substances (Gwinn et al., 2015). The current study found a similar result: $InCl_3$ induced cytotoxicity in RAW264.7 macrophages. Additionally, we demonstrated that $InCl_3$ reduced cell viability in a time-dependent manner, which reached statistical significance starting at 12 h, and in a concentration-dependent manner, which reached statistical significance starting at 1 μM. Furthermore, the cell viability was significantly reduced by $InCl_3$ incubated with RAW264.7 macrophages for 24 h compare with 12 h, but not with 48 h. Therefore, the RAW264.7 macrophages incubated with $InCl_3$ for 24 h were used on below experiments in the present study.

There are several types of cytotoxicity, including necrosis and apoptosis. Indium oxide nanocubes induce apoptosis and cytotoxicity in human lung epithelial cells (A549) (Ahamed et al., 2017). Indium nitrate and ITO nanoparticles induce apoptosis in zebrafish and its liver cells (Brun et al., 2014). Incubation of RWA264.7 cells with ITO results in apoptosis and cytotoxicity (Badding et al., 2014). In the present study, we provide the first evidence that apoptosis is induced in RAW264.7 cells incubated with $InCl_3$ in a concentration-dependent manner. Statistically significant induction of apoptosis by $InCl_3$ occurred at 1 μM. The trend of induction concentration for cytotoxicity was similar to $InCl_3$ treatment for 24 h, which induced apoptosis. By contrast, necrosis induced by $InCl_3$ treatment for 24 h significantly began at the concentration of 10 μM. These results suggested that $InCl_3$ induced cytotoxicity mostly by apoptosis rather than by necrosis.

DNA damage, also called genotoxicity, results in cytotoxicity through apoptosis (Roos and Kaina, 2013). Chemical reagents induce DNA damage through DNA lesions and DNA repair deficiency (Sirbu and Cortez, 2013; Roos and Kaina, 2013). After treatment with a mutagenic agent, whole chromosome loss, mitotic spindle damage, and unrepaired chromosome breaks lead to micronucleus formation near the nucleus following cell division (Fenech et al., 2011). Pretreatment with ITO for 24 h induced micronucleus formation in human peripheral lymphocytes (Akyıl et al., 2016). In the Chinese hamster lung cell line CHL/IU and the Chinese hamster lung fibroblast cell line V79, pretreatment with $InCl_3$ for 24 h induced micronucleus formation (Lin et al., 2013; Takagi et al., 2011). After intraperitoneal administration of $InCl_3$ for 24 h, micronuclei formed in the BALB/c mouse bone marrow (Takagi et al., 2011). In the present study, $InCl_3$ treatment for 24 h induced micronucleus formation in RAW264.7 cells in a concentration-dependent manner. Additionally, DNA single-strand breaks were detected through the alkaline comet assay. In a previous study, DNA single-strand breaks were induced by ITO and $InCl_3$ treatment for 24 h in human lung epithelial A549 cells (Tabei et al., 2016). In RAW264.7 cells, DNA single-strand breaks were induced by $InCl_3$ treatment for 24 h in a concentration-dependent manner. The

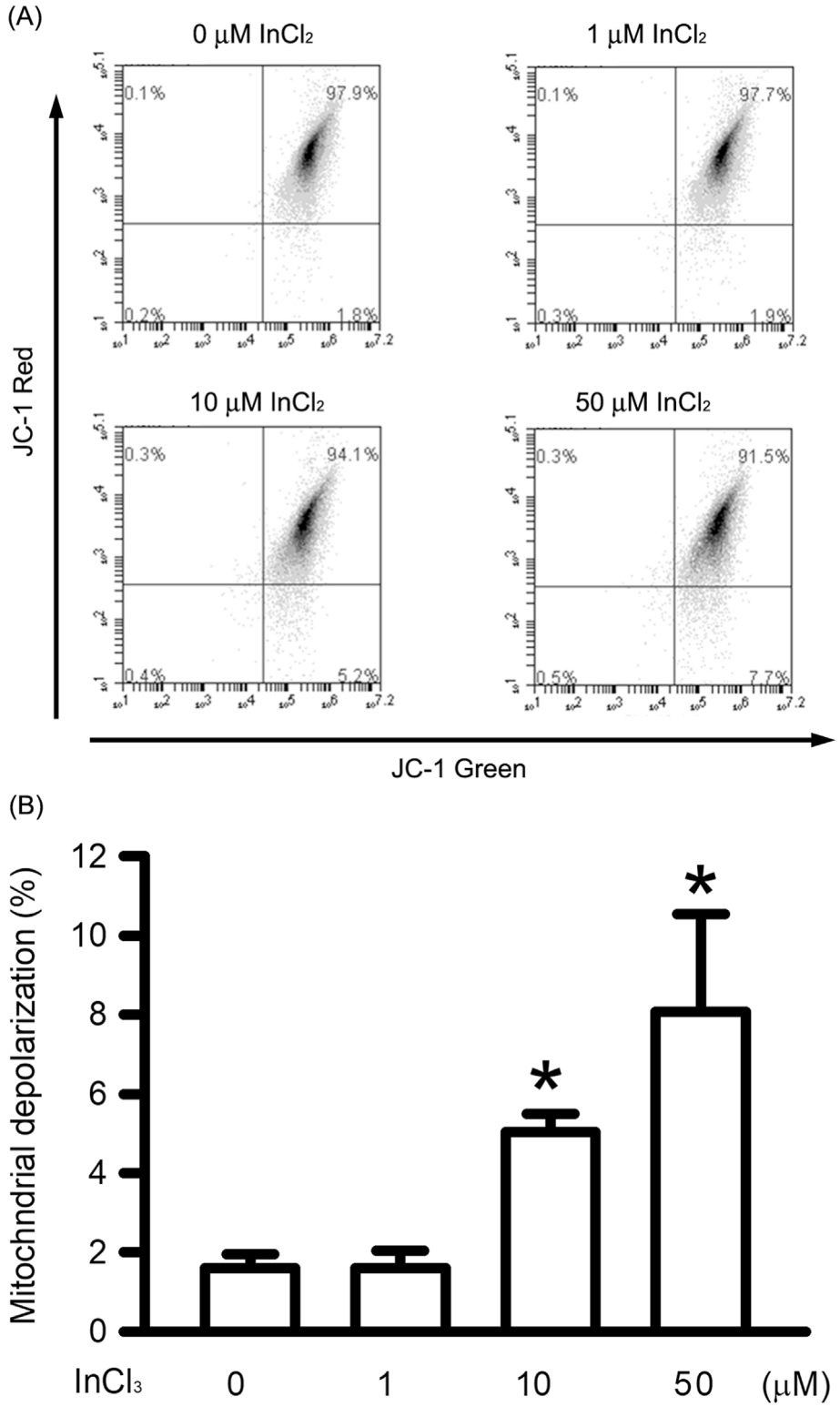

Fig. 6. $InCl_3$ induced mitochondrial dysfunction in RAW264.7 macrophages. The mitochondrial dysfunction was measured by JC-1 after treated with $InCl_3$ for 24 h at 0, 1, 10, or 50 μM. Data are expressed as mean ± SD (n = 4). *$P < 0.05$ considers significant as compare with control group, which indicated treatment with $InCl_3$ at 0 μM.

significant induction of micronucleus formation and DNA single-strand breaks by $InCl_3$ occurred at the concentration of 10 μM. The concentration at which $InCl_3$ significantly induced DNA damage was higher but similar to the concentration inducing apoptosis. These results indicated that one of the risk factors for $InCl_3$-induced apoptosis is DNA damage. However, the DNA damage also occurred in the RAW264.7 macrophages incubated solvent of $InCl_3$ treatment for 24 h. Present study used cells as mainly materials, the structure and function of replication forks when the cell cycle enters the S phase will interfere with the results of the DNA damage assay (Olive and Banáth, 2006).

Apoptosis induced by DNA damage is executed by the activation of caspase cascades. The initiator caspases include caspase-8 and -9 which

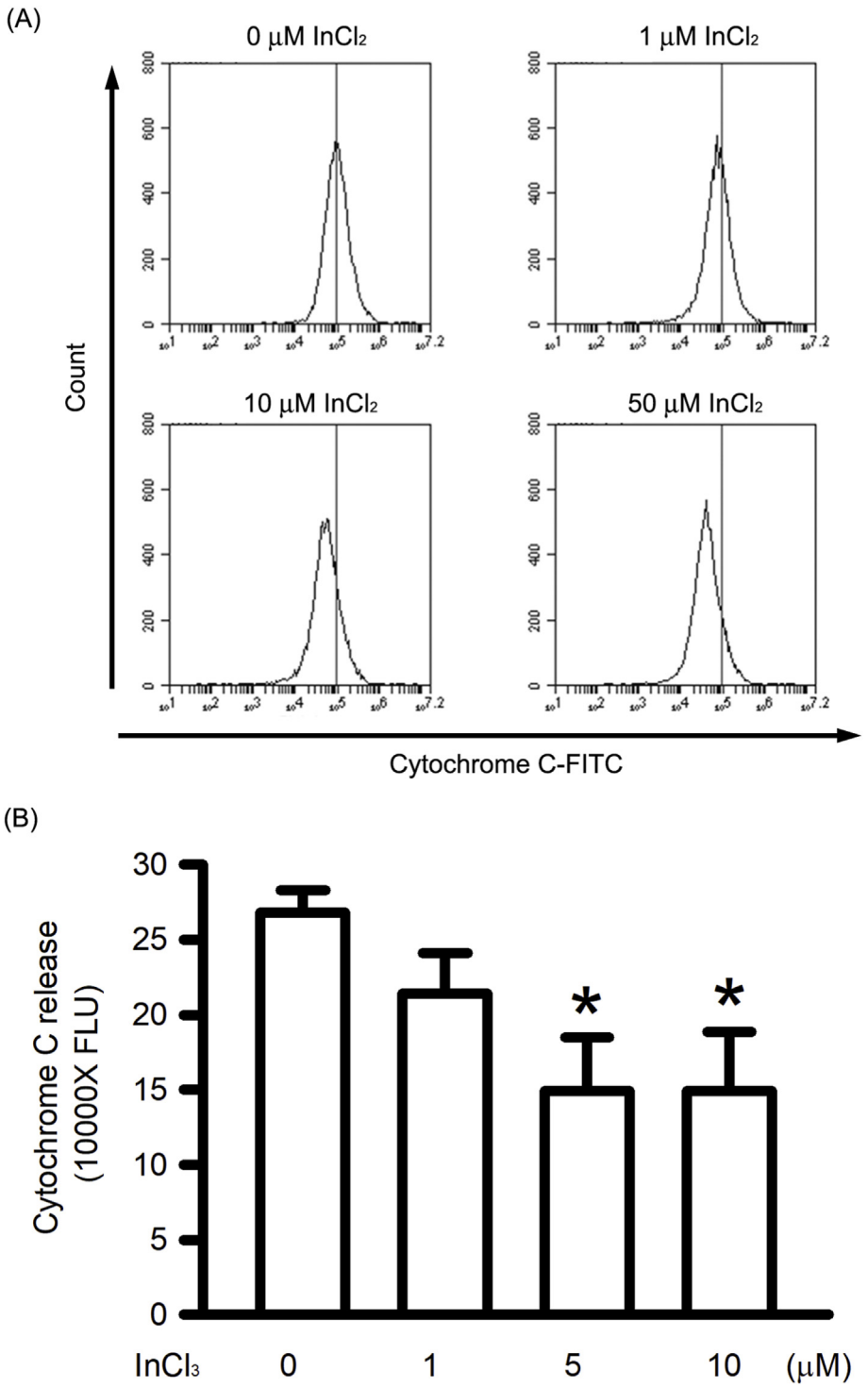

Fig. 7. $InCl_3$ induced cytochrome *c* leakage in RAW264.7 macrophages. The cytochrome *c* leakage was measured by flow cytometer. $^*P < 0.05$ considers significant as compare with control group, which indicated treatment with $InCl_3$ at 0 μM.

activated by death receptors activation and mitochondria dysfunction, respectively (Van Opdenbosch and Lamkanfi, 2019). The effector caspases, such as caspase-3, is performed by the activated initiator caspases. Activation of caspase-3 induces the dimerization of caspase-activated DNase and the cleavage of poly-ADP-ribose polymerase, which then result in apoptosis through DNA damage (Kitazumi and Tsukahara, 2011; Norbury and Zhivotovsky, 2004). In A549 cells, caspase-3 and -9 activities were induced by indium oxide nanocubes (Ahamed et al., 2017). In the present study, we first showed that the activities of caspase-3, -8, and -9 were upregulated in RAW264.7 cells treated with $InCl_3$ for 24 h in a concentration-dependent manner. Furthermore, mitochondrial dysfunction is the key mediator of caspase activation (Wang and Youle, 2009). Yuan et al. (2017) proposed that isolated mitochondrial permeability transition is induced by indium (III) through the reduction of proton channels located in the inner membrane. The destruction of mitochondria and the production of testosterone were found in the Leydig cells of mature male Wistar rats after treatment with indium nitrate (Samira et al., 2011). In the present

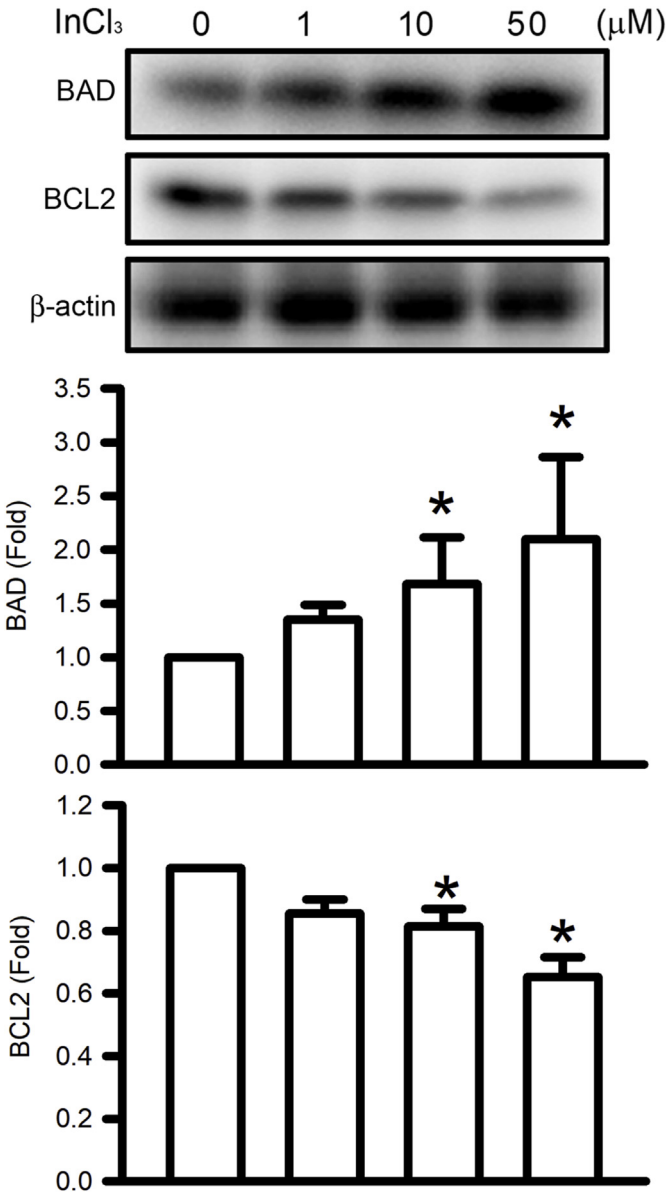

Fig. 8. Effect of $InCl_3$ on BAD and BCL2 expression in RAW264.7 macrophages. The expression of BAD and BCL2 was measured by Western blot assay. *$P < 0.05$ considers significant as compare with control group, which indicated treatment with $InCl_3$ at 0 μM.

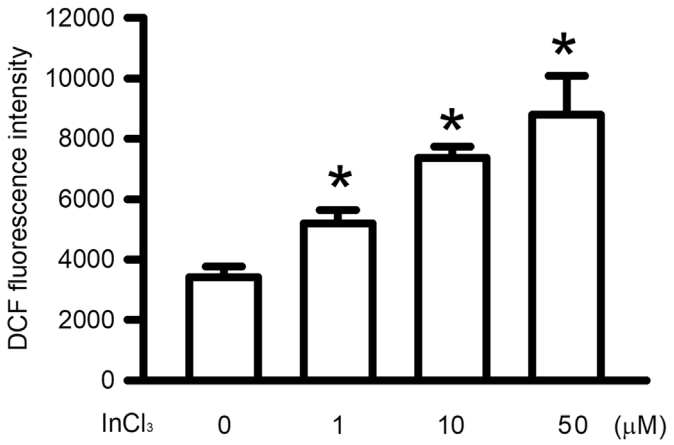

Fig. 9. $InCl_3$ induced generation of ROS in RAW264.7 macrophages. The generation of ROS was measured by DCFH-DA after treated with $InCl_3$ for 24 h at 0, 1, 10, or 50 μM respectively. Data are expressed as mean ± SD (n = 4). *$P < 0.05$ considers significant as compare with control group, which indicated treatment with $InCl_3$ at 0 μM.

study, we demonstrated that $InCl_3$ induced mitochondrial dysfunction in RAW264.7 cells, which was significantly induced after 10 μM $InCl_3$ treatment for 24 h. The effect of $InCl_3$ on mitochondrial dysfunction and its downstream factors, including caspase-3, -8, and -9, showed a similar concentration trend as DNA damage for RAW264.7 cells treated with $InCl_3$. These results indicated $InCl_3$ induced DNA damage through caspase-3, -8, -9, and their upstream factor, mitochondrial dysfunction.

Cytochrome *c* release from the mitochondria and mitochondrial depolarization, caused by an increased permeability of the mitochondrial membrane, play major roles in the mitochondria-dependent apoptotic pathway (Bernardi et al., 2015). The downregulation of BCL2 and upregulation of BAD led to the activation of BAX and Bak and subsequently provoked the permeability of the mitochondrial membrane (Borner and Andrews, 2014). In A549 cells, the downregulation of BCL2 and upregulation of BAX were induced by indium oxide nanocubes (Ahamed et al., 2017). Based on the primary results of the present study, we proposed that RAW264.7 cell treatment with $InCl_3$ for 24 h resulted in leakage of cytochrome *c* from the mitochondria, downregulation of BCL2 expression, and upregulation of BAD expression in a concentration-dependent manner. These results indicated that $InCl_3$ induced mitochondrial dysfunction through cytochrome *c* leakage and the alteration of BAD and BCL2 expression.

Intracellular ROS are crucial signaling molecules for mitochondrial dysfunction, DNA damage, and apoptosis (Redza-Dutordoir and Averill-Bates, 2016). In normal conditions, intracellular ROS are generated by normal cellular metabolism, including xanthine oxidase, cytochrome P450, cyclooxygenase, and the electron transfer system (Abdal Dayem et al., 2017). However, tissue damage, gene mutation, and toxic effects are induced by overproduction of ROS caused by extracellular risk factors, such as carcinogens, mutagens, and air pollutants (Moloney and Cotter, 2018). Indium (III) triggers ROS production in isolated mitochondria (Yuan et al., 2017). During sexual maturation, $InCl_3$ increased ROS generation within sperm in a rodent model (Lee et al., 2015). ROS generation was also induced by ITO in A549 cells and RAW264.7 cells (Tabei et al., 2018; Olgun et al., 2017; Ahamed et al., 2017). Based on the results of the present study, the generation of intracellular ROS was induced by $InCl_3$ in a concentration-dependent manner. These results indicated that $InCl_3$ induced mitochondrial dysfunction, DNA damage, and apoptosis through intracellular ROS generation.

In conclusion, $InCl_3$ induced cytotoxicity in RAW264.7 macrophages through apoptosis but not through necrosis. The mechanism of $InCl_3$-induced apoptosis involved DNA damage and its upstream factors, including caspase-3, -8, and -9 activation. $InCl_3$-induced upregulation of caspase activity was mediated by mitochondrial dysfunction through cytochrome *c* leakage and by alteration of BAD and BCL2 expression. Finally, the generation of ROS played the most important role in mitochondrial dysfunction, genotoxicity, and apoptosis induced by $InCl_3$. According to the current findings, we first proposed the mechanism of $InCl_3$-induced toxic effects on macrophages. This information could be used to avoid damage caused by indium among industrial workers.

CRediT authorship contribution statement

Ping-Kun Tsai: Conceptualization, Methodology, Formal analysis, Investigation, Resources, Writing - original draft, Funding acquisition. **Sheng-Wen Wu:** Methodology, Software, Investigation, Data curation, Writing - original draft. **Chen-Yu Chiang:** Methodology, Software, Investigation, Writing - original draft. **Min-Wei Lee:** Methodology,

Formal analysis. **Hung-Yi Chen:** Methodology, Formal analysis. **Wen-Ying Chen:** Software, Validation, Resources, Funding acquisition. **Chun-Jung Chen:** Software, Validation, Writing - original draft. **Shun-Fa Yang:** Conceptualization, Validation, Resources, Writing - review & editing. **Chao-Bin Yeh:** Conceptualization, Software, Investigation, Resources, Writing - review & editing, Supervision. **Yu-Hsiang Kuan:** Conceptualization, Software, Investigation, Writing - review & editing, Supervision, Funding acquisition.

Declaration of competing interest

All authors declare no conflict of interest.

Acknowledgments

The authors would like to thank the Ministry of Science and Technology of the Republic of China for financially supporting this research under Contract No. MOST 105-2320-B-040-022- and 106-2320-B-040-022-MY3. We also thank the Zuoying Branch of Kaohsiung Armed Forces General Hospital under Grant No. ZBH 107–02 and the National Chung Hsing University and Chung Shan Medical University (NCHU-CSMU-10503810) for financially supporting this research. This manuscript was edited by Wallace Academic Editing.

References

Abdal Dayem, A., et al., 2017. The role of reactive oxygen species (ROS) in the biological activities of metallic nanoparticles. Int. J. Mol. Sci. 18, E120.
Ahamed, M., et al., 2017. Nanocubes of indium oxide induce cytotoxicity and apoptosis through oxidative stress in human lung epithelial cells. Colloids Surf. B Biointerfaces 156, 157–164.
Akyıl, D., et al., 2016. Determination of mutagenicity and genotoxicity of indium tin oxide nanoparticles using the Ames test and micronucleus assay. Toxicol. Ind. Health 32, 1720–1728.
Badding, M.A., et al., 2015. Sintered indium-tin oxide particles induce pro-inflammatory responses in vitro, in part through inflammasome activation. PloS One 10, e0124368.
Badding, M.A., et al., 2014. Cytotoxicity and characterization of particles collected from an indium-tin oxide production facility. J. Toxicol. Environ. Health A. 77, 1193–1209.
Bernardi, P., et al., 2015. The mitochondrial permeability transition pore: channel formation by F-ATP synthase, integration in signal transduction, and role in pathophysiology. Physiol. Rev. 95, 1111–1155.
Bomhard, E.M., 2018. The toxicology of indium oxide. Environ. Toxicol. Pharmacol. 58, 250–258.
Borner, C., Andrews, D.W., 2014. The apoptotic pore on mitochondria: are we breaking through or still stuck? Cell Death Differ. 21, 187–191.
Brun, N.R., et al., 2014. Indium and indium tin oxide induce endoplasmic reticulum stress and oxidative stress in zebrafish (Danio rerio). Environ. Sci. Technol. 48, 11679–11687.
Chen, Z., et al., 2019. The pneumotoxic effect and indium ion release induced by indium tin oxide nanoparticles. J. Nanosci. Nanotechnol. 19, 4357–4365.
Chien, K.J., et al., 2018. Safrole induced cytotoxicity, DNA damage, and apoptosis in macrophages via reactive oxygen species generation and Akt phosphorylation. Environ. Toxicol. Pharmacol. 64, 94–100.
Chonan, T., et al., 2019. Indium lung: discovery, pathophysiology and prevention. Tohoku J. Exp. Med. 248, 143–150.
Fenech, M., et al., 2011. Molecular mechanisms of micronucleus, nucleoplasmic bridge and nuclear bud formation in mammalian and human cells. Mutagenesis 26, 125–132.
Gwinn, W.M., et al., 2015. Macrophage solubilization and cytotoxicity of indium-containing particles as in vitro correlates to pulmonary toxicity in vivo. Toxicol. Sci. 144, 17–26.
Gwinn, W.M., et al., 2013. Macrophage solubilization and cytotoxicity of indium-containing particles in vitro. Toxicol. Sci. 135, 414–424.
Hasegawa, G., et al., 2012. Differential genotoxicity of chemical properties and particle size of rare metal and metal oxide nanoparticles. J. Appl. Toxicol. 32, 72–80.
Hines, C.J., et al., 2013. Use of and occupational exposure to indium in the United States. J. Occup. Environ. Hyg. 10, 723–733.
Huang, F.M., et al., 2018. Bisphenol A exhibits cytotoxic or genotoxic potential via oxidative stress-associated mitochondrial apoptotic pathway in murine macrophages. Food Chem. Toxicol. 122, 215–224.
Huang, F.M., et al., 2019. Expression of pro-inflammatory cytokines and mediators induced by Bisphenol A via ERK-NFκB and JAK1/2-STAT3 pathways in macrophages. Environ. Toxicol. 34, 486–494.
Kitazumi, I., Tsukahara, M., 2011. Regulation of DNA fragmentation: the role of caspases and phosphorylation. FEBS J. 278, 427–441.
Lee, C.Y., et al., 2018. Cadmium nitrate-induced neuronal apoptosis is protected by N-acetyl-l-cysteine via reducing reactive oxygen species generation and mitochondria dysfunction. Biomed. Pharmacother. 108, 448–456.
Lee, K.H., et al., 2015. Effects of indium chloride exposure on sperm morphology and DNA integrity in rats. J. Food Drug Anal. 23, 152–160.
Li, Y., et al., 2011. Recovery of indium from used indium–tin oxide (ITO) targets Hydrometallurgy 105, 207–212.
Lin, R.H., et al., 2013. Indium chloride-induced micronuclei via reactive oxygen species in Chinese hamster lung fibroblast V79 cells. Environ. Toxicol. 28, 595–600.
Lison, D., 2009. Sintered indium-tin-oxide (ITO) particles: a new pneumotoxic entity. Toxicol. Sci. 108, 472–481.
Moloney, J.N., Cotter, T.G., 2018. ROS signalling in the biology of cancer. Semin. Cell Dev. Biol. 80, 50–64.
Nagano, K., et al., 2011. Inhalation carcinogenicity and chronic toxicity of indium-tin oxide in rats and mice. J. Occup. Health 53, 175–187.
Norbury, C.J., Zhivotovsky, B., 2004. DNA damage-induced apoptosis. Oncogene 23, 2797–2808.
Olgun, N.S., et al., 2017. Comparison of the toxicity of sintered and unsintered indium-tin oxide particles in murine macrophage and epidermal cells. Toxicol. Appl. Pharmacol. 331, 85–93.
Olivares, C.I., et al., 2016. Arsenic (III, V), indium (III), and gallium (III) toxicity to zebrafish embryos using a high-throughput multi-endpoint in vivo developmental and behavioral assay. Chemosphere 148, 361–368.
Olive, P.L., Banáth, J.P., 2006. The comet assay: a method to measure DNA damage in individual cells. Nat. Protoc. 1, 23–29.
Phipps, G., et al., 2008. Indium and gallium: long-term supply Renew. Energy Focus 9, 56–59.
Redza-Dutordoir, M., Averill-Bates, D.A., 2016. Activation of apoptosis signalling pathways by reactive oxygen species. Biochim. Biophys. Acta 1863, 2977–2992.
Roos, W.P., Kaina, B., 2013. DNA damage-induced cell death: from specific DNA lesions to the DNA damage response and apoptosis. Canc. Lett. 332, 237–248.
Samira, M., et al., 2011. Histological and ultrastructural study of the intracellular behavior of indium in the testicular tissues. Microsc. Res. Tech. 74, 546–550.
Sirbu, B.M., Cortez, D., 2013. DNA damage response: three levels of DNA repair regulation. Cold Spring Harb. Perspect. Biol. 5, a012724.
Tabei, Y., et al., 2016. Intracellular accumulation of indium ions released from nanoparticles induces oxidative stress, proinflammatory response and DNA damage. J. Biochem 159, 225–237.
Tabei, Y., et al., 2018. Reactive oxygen species independent genotoxicity of indium tin oxide nanoparticles triggered by intracellular degradation. Food Chem. Toxicol. 118, 264–271.
Takagi, R., et al., 2011. Indium chloride-induced micronuclei in in vivo and in vitro experimental systems. J. Occup. Health 53, 102–109.
Tanaka, A., et al., 2010. Chronic pulmonary toxicity study of indium-tin oxide and indium oxide following intratracheal instillations into the lungs of hamsters. J. Occup. Health 52, 14–22.
Van Opdenbosch, N., Lamkanfi, M., 2019. Caspases in cell death, inflammation, and disease. Immunity 50 1352–1136.
Wang, C., Youle, R.J., 2009. The role of mitochondria in apoptosis. Annu. Rev. Genet. 43, 95–118.
Wang, H., 2011. The effect of the proportion of thin film transistor-liquid crystal display (TFT-LCD) optical waste glass as a partial substitute for cement in cement mortar. Construct. Build. Mater. 25, 791–797.
Yuan, L., et al., 2017. Indium (III) induces isolated mitochondrial permeability transition by inhibiting proton influx and triggering oxidative stress. J. Inorg. Biochem. 177, 17–26.
Zhang, K., et al., 2015. Recycling indium from waste LCDs: a review. Resour. Conserv. Recycl. 104, 276–290.